Anisotropic Interaction and Stereoreactivity in a Chemi-Ionization Process of OCS by Collision with He*(2^3S) Metastable Atoms

Takuya Horio, Satoshi Maeda, Naoki Kishimoto, and Koichi Ohno*

Department of Chemistry, Graduate School of Science, Tohoku University, Aramaki, Aoba-ku, Sendai, 980-8578, Japan

Received: June 17, 2006; In Final Form: August 4, 2006

Ionic-state-resolved collision energy dependence of Penning ionization cross sections for OCS with He*-(2^3S) metastable atoms was measured in a wide collision energy range from 20 to 350 meV. Anisotropic interaction potential for the OCS−He*(2^3S) system was obtained by comparison of the experimental data with classical trajectory simulations. It has been found that attractive potential wells around the O and S atoms are clearly different in their directions. Around the O atom, the collinear approach is preferred (the well depth is ca. 90 meV), while the perpendicular approach is favored around the S atom (the well depth is ca. 40 meV). On the basis of the optimized potential energy surface and theoretical simulations, stereo reactivity around the O and S atoms was also investigated. The results were discussed in terms of anisotropy of the potential energy surface and the electron density distribution of molecular orbitals to be ionized.

1. Introduction

In collisional reactions of molecules, it is important to investigate structural and steric factors of the colliding system, such as the relative orientation of the reactants, since they decisively affect the reaction rate constant. In this point of view, stereodynamics has been one of the key subjects in recent molecular physics and chemistry.[1,2] Experimental techniques for controlling the orientation or alignment of molecules, such as an electric hexapole state selector[3−5] or collisional alignment of molecular rotations in seeded supersonic molecular beams,[6−9] have been established to investigate stereodynamical effects in reactive or nonreactive scattering collisions.

Stereodynamics of the reactions between excited rare gas atoms and small molecules has also been studied, partly because one of the reaction channels is an unique chemiionization process known as Penning ionization,[10] which is characterized by the electron exchange model.[11] The ionization occurs when a molecule M collides with a metastable rare gas atom A* having an excitation energy larger than the ionization potential (IP) of M,

$$A^* + M \rightarrow M_i^+ + A + e^- \qquad (1)$$

According to the electron exchange model,[11] the reaction probability producing different ionic states of M (M_i^+) depends on the mutual overlap between the molecular orbital (MO) ϕ to be ionized and the inner vacant orbital χ of A*, because an electron is transferred from ϕ to χ followed by ejection of an electron from the outer orbital in A*. Experimental branching ratios for each ionic state of M_i^+ obtained by Penning ionization electron spectroscopy (PIES)[12,13] are found to be related to the electron density outsides the repulsive boundary surface of the target molecule.[14,15] Therefore, Penning ionization has been regarded as a sensitive probe for the electron density distribution of MOs to be ionized. From the standpoint of this remarkable feature, studies of stereoreactivity in Penning ionization have been performed in some groups. The steric dependence in two competing reaction channels of Penning ionization and neutral dissociation for the system of CS_2 + Ar*(^{3}P) was studied utilizing a laser photodissociation method for preparing a large amount of aligned CS_2 molecules in the effusive molecular beam.[16] An electrostatic hexapole field for selecting rotational states of polar molecules with first-order Stark effect have also been employed to study the steric effects in several colliding systems of Ar*(^{3}P) with methyl halide molecules.[17−19]

Another kind of experimental study to investigate stereodynamics in collisional ionization of molecules utilizes an electron spectroscopic technique combined with a time-of-flight (TOF) method for velocity selections of A*. Since the spatial distribution of the electron density for each MO is usually highly anisotropic, "partial" Penning ionization cross sections σ_i are expected to provide information on collisional ionization in the specific region where the electron density of a MO spatially distributes, even though target molecules are randomly oriented in the laboratory frame. Further, velocity selections of A* allow us to gain energy dependence of Penning ionization cross sections and to study stereo reaction dynamics upon the interaction potential V^* for the A*−M system. The first measurement of collision energy dependence of partial ionization cross sections (CEDPICS) for molecular targets was performed with a high flux He*(2^3S) (excitation energy = 19.82 eV) atomic beam.[20−22] CEDPICS has provided a straightforward investigation on anisotropy of V^* as well as on stereodynamics in collisional ionization of various molecules.[23]

Theoretical studies on stereodynamics in collisional ionization of molecules have also been carried out on the basis of the theory of Penning ionization, where the ionization width and the interaction potentials are needed to understand the ionization dynamics.[24,25] Semiempirical treatments have been employed for the systems of Ne*($^3P_{0,2}$) + CH_3Cl and He*($2^{3,1}$S),[26] Ne*-($^3P_{0,2}$) + N_2O[27] in order to investigate anisotropic effect in collisional ionization. On the other hand, CEDPICS for molecular targets was first calculated by classical trajectory simulations

* Corresponding author. Telephone: +81-22-795-6576. Fax: +81-22-795-6580. E-mail: ohnok@qpcrkk.chem.tohoku.ac.jp.

10.1021/jp0637781 CCC: $33.50 © 2006 American Chemical Society
Published on Web 09/06/2006

based on ab initio interaction potentials and approximated ionization widths.[28,29] Reliable potentials for molecular targets, however, have not been obtained by ab initio treatment, because of difficulties in constructing highly anisotropic interaction of A* + M systems embedded in an ionization continuum higher than the IP of M. To compare the calculated results with the observed ones quantitatively, interaction potentials employed in trajectory calculations need to be modified based on an optimization procedure. An overlap expansion method improving anisotropic potential has been developed very recently,[30] and then for several targets, such as N_2,[30] CO,[30] CH_3CN,[31] C_2H_2,[32] C_2H_4,[32] and C_6H_6,[33] spatial anisotropy of V^* with He*-(2^3S) and stereodynamics of the collisional ionization upon V^* has been investigated in detail.

Here, we report a joint experimental and theoretical study for a target molecule having two heteroatoms; carbonyl sulfide OCS. A Penning ionization electron spectrum of OCS was recorded by Čermák[34] and Brion and Yee,[35] who observed a large band intensity of the $C^2\Sigma^+$ ionic state of OCS^+. From our previous studies for NH_2CXNH_2[36] and CH_3CXNH_2 (X = O and S),[37] interestingly an attractive well of the interaction potential V^* was found to be in perpendicular directions around the C═S axis, while collinear direction of the C═O axis was the most attractive site around the O atom. Since the above studies were mainly based on experimental investigations, comparative studies with theoretical simulations for the observed results are necessary in order to gain more detailed information on collisional reaction dynamics and anisotropic interaction around the O and S atoms. CEDPICS of OCS was observed in the energy range from 80 to 250 meV,[38] however, a lack of experimental data in lower collision energies (<80 meV) has made it difficult to evaluate the interaction potential V^* accurately (for example, the position of the attractive site and the well depth).

In this work, by means of a liquid N_2 cooled discharge source for He*(2^3S) metastable beams,[31] CEDPICS of OCS has been recorded in a wide collision energy range from 20 to 350 meV. Interaction potential V^* for the present system has been obtained by the experimental data and the theoretical methods mentioned above. In addition, stereo reaction dynamics of collisional ionization of OCS is investigated based on the optimized potential.

II. Experimental Section

Details of the experimental setup were reported previously.[31,32] The apparatus consists of four differentially pumped vacuum chambers. Metastable atoms of He*(2^1S, 2^3S) were produced by a nozzle discharge source with a tantalum hollow cathode and a grounded conical skimmer (throat diameter = 0.7 mm). A machined piece of boron nitride (BN) nozzle (orifice diameter = 0.8 mm) was attached onto a Pyrex glass pipe for introducing helium gas (purity >99.99995%). For experiments in lower collision energies, this nozzle cap can be cooled to ca. 180 K by a liquid N_2 circulator. A mechanical chopper (100 mm diameter, 0.2 mm thick) with a slit width of 2 mm was used for TOF measurements of the metastable helium beams. The He*(2^1S) components in the beam were optically quenched by a water-cooled He discharge lamp. Gaseous OCS was introduced directly into the ionization region from an effusive beam nozzle. The sample was commercially purchased and used without further purification. The base pressure in the reaction chamber was about 3×10^{-8} Torr, and measurements were performed under the pressure of 1.5×10^{-6} Torr with both beams on. An electrostatic retarding-type analyzer equipped with a magnetic bottle[39] was used for measurements of the kinetic energy distribution of the ejected electrons. The ejected electrons were decelerated by the retarding electrodes, and then accelerated to the former speed. Electrons passed through the retarding fields were detected by a dual microchannel plate placed at the end of the flight tube.

Electron signals as functions of electron kinetic energy (E_e) and TOF of the He*(2^3S) atoms between the collision center and the chopper disk $I_e(E_e, t)$ were recorded in a two-parameter multichannel scaler equipped with a retarding voltage generator (Laboratory Equipment Corporation, VSCANMCS NT-2400 M).[40] A typical time resolution, a step of electron-energy scans, and a dwell-time were 2 μs, 40 meV, and 100 ms, respectively. The $I_e(E_e, t)$ can be converted to $I_e(E_e, v_{He^*})$ as functions of E_e and velocity of metastable He* atoms (v_{He^*}). The two-dimensional Penning ionization cross section $\sigma(E_e, v_r)$ was obtained by normalization with the velocity distribution of He* atoms I_{He^*} (v_{He^*}):

$$\sigma(E_e, v_r) = c\frac{I_e(E_e, v_{He^*})}{I_{He^*}(v_{He^*})}\frac{v_{He^*}}{v_r} \tag{2}$$

$$v_r = \sqrt{{v_{He^*}}^2 + \frac{3k_BT}{m_M}} \tag{3}$$

where c is a constant, v_r is the relative velocity between the He*(2^3S) atom and the target molecule (OCS) under an effusive beam condition, k_B is the Boltzmann constant, T is the temperature of the effusive nozzle (room temperature), and m_M is the mass of OCS molecule. $I_{He^*}(v_{He^*})$ was obtained by monitoring secondary electrons emitted from an inserted stainless steel needle. It should be noted that TOF of the ejected electrons to reach the electron detector (MCP) from the ionization region (<0.5 μs) can be negligible in comparison with that of the metastable He*(2^3S) atoms to reach the collision center from the chopper disk (200−800 μs). Finally, $\sigma(E_e, v_r)$ is converted to the final form $\sigma(E_e, E_c)$:

$$E_C = \frac{1}{2}\mu{v_r}^2 \tag{4}$$

where μ is the reduced mass of the colliding system.

III. Calculations

In the present study, classical trajectory calculations on a three-dimensional potential were performed in order to obtain CEDPICS theoretically. A full description of the method of calculations was reported previously.[30−33] Since it has been still a difficult problem to obtain interaction potentials containing metastable rare gas atoms in good accuracy as mentioned in section I, first we started from calculating an approximate interaction potential $V_0(R, \theta)$ using Li(2^2S) in place of He*-(2^3S) on the basis of the well-known resemblance between He*-(2^3S) and Li(2^2S)[41−44] ($V_0(R, \theta)$: Li model potential). Here, R is the distance between the Li atom and the center of mass of OCS and θ denotes the polar angle from the molecular axis ($0° \le \theta \le 180°$). Ab initio MO calculations of V_0 for the OCS + Li system were performed on a GAUSSIAN quantum chemistry program[45] at the coupled cluster level of theory including single, double, and optional triple excitation CCSD(T) with 6-311+G* basis set. The ab initio interaction energies were calculated at 169 independent sampling points, 12−15 points of different R and every 15° of θ. The basis-set super position error (BSSE) in calculating V_0 was corrected by the full counterpoise method.[46]

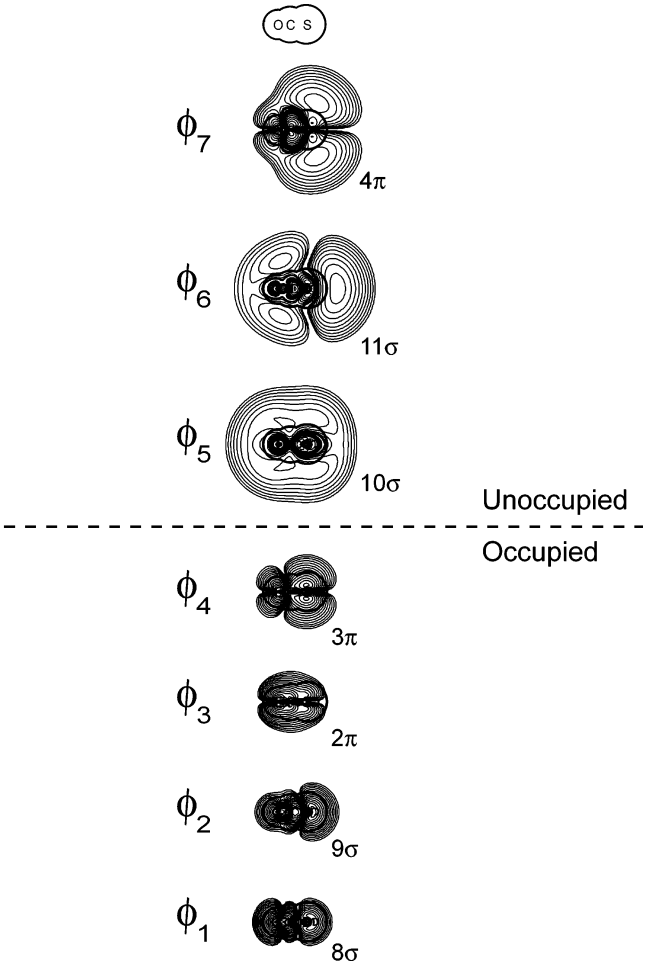

Figure 1. Contour maps of the electron density of MOs for OCS. Occupied MOs (8σ, 9σ, 2π, and 3π,) and unoccupied MOs (10σ, 11σ, and 4π) were used for optimizations of potential energy surface (see text). The thick solid line in the contour maps represents the molecular surface of OCS estimated approximately from van der Waals radii of component atoms in order to show the molecular shape schematically.

For the purpose of obtaining better agreement with experimental results and evaluating the interaction potential for the present system accurately, the Li model potential V_0 should be modified by a reasonable manner as mentioned in section I. It is easily recognized that an excited 2s electron of He*(2^3S) mainly contributes to the interaction with M, and the orbital interaction between Li(2^2S) and M should differ to some extent from those of He*(2^3S). Thus, it is reasonable to modify V_0 according to the overlap between the relevant orbitals. In the present study, the overlap expansion (OE) method improving three-dimensional potentials[30] has been employed. In the OE method, calculated V_0 can be modified by the following equations to give $V^*(R, \theta)$ for He*(2^3S):

$$V^*(R, \theta) = V_0(R, \theta) - \sum_i C_i |\langle \phi_i | \chi \rangle|^2 \tag{5}$$

$$\chi = \sqrt{\zeta^3/\pi}\, \exp[-\zeta r] \tag{6}$$

Here, χ is a Slater-type *s* orbital function with an exponent ζ, which is located at the position of the He*/Li atom. *r* is the distance from the center of χ. As described previously,[30] the OE method is able to describe effectively anisotropic potentials by expanded terms using overlap integrals between target MOs ϕ_i and an atomic orbital χ. The expansion coefficients C_i in eq 5 and the exponent ζ in eq 6 are parameters to be optimized in the potential corrections; however, in our previous studies[30−33] the optimized values of ζ in eq 6 have been found to be very close to the exponent of the 2s orbital of He* atom, which is 0.575 bohr^{-1} determined by Slater's rule. According to this fact, the parameter of ζ was fixed at the above value.

In trial calculations for the optimization procedure based on eq 5, it was found that the following MOs ϕ_i should be included in the correction term: 8σ, 9σ, 2π, 3π, 10σ, 11σ, and 4π orbitals. Electron density contour maps of the respective MOs with the numbering of ϕ_i and C_i are shown in Figure 1. The molecular shape estimated from van der Waals radii of O, C, and S are shown schematically with thick solid lines. The MOs were obtained by ab initio self-consistent field (SCF) calculations with 6-311+G** basis set.

Classical trajectory calculations on $V^*(R, \theta)$ ($V_0(R, \theta)$) were performed to simulate CEDPICS in the studied collision energy range. The relative motion of the colliding system was determined by solving the equation of motion. During collisions, the molecular structure was fixed at the experimental geometry. Concerning this treatment, we have found that the observed Penning ionization electron spectrum of OCS is well correlated to the He(I) ultraviolet photoelectron spectrum (UPS) except for the branching ratio. Small (<50 meV) peak energy shifts (difference between the observed kinetic energy in PIES and the "nominal" energy E_0 (=19.82 − IP)) are confirmed experimentally,[38] which indicates that structural deformation leading to a strong attractive interaction between He* and OCS is considered to be unlikely. Thus, the approximation of the frozen molecular structure is reasonable in the present trajectory calculations. The molecular orientation and the rotational angular momentum vector were randomly generated, and then the initial rotational energy was made so that the distribution obeys Boltzmann distribution at room temperature to match the experimental condition. The impact parameter *b* was also generated randomly from 0 to 8 Å. For a given collision energy E_c, calculations of 10 000 trajectories with the above initial parameters were performed.

On the basis of the discussion noted previously,[30−33] the ionization width $\Gamma^{(i)}$ producing each ionic state of OCS^+ was evaluated in the following manner;

$$\Gamma^{(i)} = K^{(i)} |\langle \phi_i | \chi_{1s} \rangle|^2 \tag{7}$$

where $K^{(i)}$ is a parameter to be determined so as to reproduce observed branching ratio and collision energy dependence for respective ionic states. This treatment is based on the consideration that $\Gamma^{(i)}$ is mainly governed by the mutual overlap between the He 1s orbital (χ_{1s}) and corresponding MOs (ϕ_i). This treatment allows us to avoid theoretical and computational difficulties associated with direct calculations of the matrix elements including highly excited states for too many geometrical configurations. The orbital functions for the target molecules and a He atom in eq 7 were obtained by SCF calculations with 6-311+G* basis set.

At each trajectory step of an interval d*t*, transition probabilities $P^{(i)}(t)\, \mathrm{d}t$ into each ionic state *i* can be expressed by

$$P^{(i)}(t)\, \mathrm{d}t = S(t)\, \frac{\Gamma^{(i)}}{\hbar}\, \mathrm{d}t \tag{8}$$

$$S(t) = 1 - \sum_i P^{(i)}_{\mathrm{int}}(t) \tag{9}$$

where the survival fraction $S(t)$ is the probability of He*(2^3S) surviving in the excited state at a certain time *t* and then $P^{(i)}_{\mathrm{int}}$

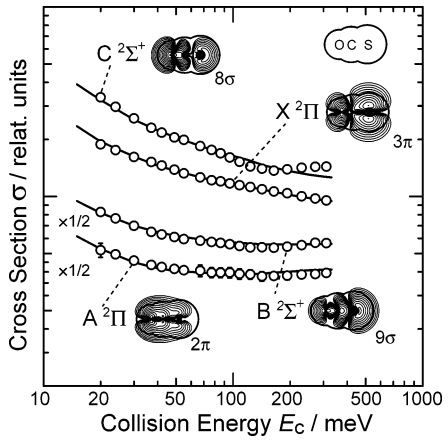

Figure 2. Observed log σ(cross section) − log E_c(collision energy) plots of CEDPICS for OCS are shown with circles in the collision energy range from 20 to 350 meV. Solid lines represent calculated CEDPICS obtained by the classical trajectory calculations on the optimized potential V^*. The calculated electron density contour maps of SCF-MOs corresponding to the relevant ionic states are also shown.

represents the integrated partial ionization probability before time t. Finally, the partial ionization cross section $\sigma^{(i)}$ was obtained from the partial ionization probability $P^{(i)}$ of a trajectory:

$$\sigma^{(i)} = \int_0^\infty 2\pi b P^{(i)}\, db \qquad (10)$$

Since ionization probabilities depend not only on the impact parameter b but also on the molecular rotational motion and orientation, many different situations are involved in the same impact parameter. In section IV.C, this will be discussed in detail.

Parameters of C_i and $K^{(i)}$ in eqs 5 and 7 were optimized by a nonlinear least-squares fitting method in order to reproduce the slopes and branching ratios in the observed CEDPICS. The optimization of the slope of CEDPICS and branching ratio was performed at the calculated points for the collision energy E_c of 20, 50, 100, 150, and 300 meV.

IV. Results and Discussion

A. Characteristic Features of CEDPICS. PIES and He(I) UPS of OCS were reported in the previous paper.[38] Valence ionic states of OCS have been studied for a long time by experimental methods such as photoelectron spectroscopy,[34,35,47−51] electron impact ionization,[52] and Penning ionization electron spectroscopy.[34,35] Theoretical calculations were also made to assign the produced ionic states of OCS.[53,54] Two $^2\Pi$ ionic states denoted by $X^2\Pi$ and $A^2\Pi$ were produced by collision with He*-(2^3S) metastable atoms (excitation energy = 19.82 eV). $X^2\Pi$ ionic state can be ascribed to ionization from 3π molecular orbital (MO) having an antibonding character ($S_{3p} - O_{2p}$), while $A^2\Pi$ ionic state corresponds to ionization from 2π (π_{CO}) MO with a bonding character ($C_{2p} + O_{2p}$). For ionization from σ orbitals, two $^2\Sigma^+$ ionic states were produced. $B^2\Sigma^+$ and $C^2\Sigma^+$ ionic states can be ascribed to ionization from 9σ MO with S_{3s} character and 8σ MO with σ_{CO} character, respectively.

Figure 2 shows the observed log σ (cross section) − log E_c (collision energy) plots of CEDPICS (open circles) for OCS in the collision energy range from 20 to 350 meV. The calculated electron density contour maps of SCF-MOs corresponding to the relevant ionic states are also shown. The observed slope parameters m for log σ vs log E_c plots in collision energy regions of 20−50, 50−100, and 100−310 meV are summarized in Table 1. The values of m were obtained by a least-squares method. Figure 2 also compares the observed CEDPICS with the calculated CEDPICS obtained by classical trajectory calculations on the optimized V^*. From the comparison of the observed CEDPICS with the calculated CEDPICS, it can be said that present trajectory calculations using the optimized V^* well account for the observed features of CEDPICS in the studied collision energy range.

TABLE 1: Slope Parameters m of the Observed CEDPICS for OCS + He*(2^3S) in the Collision Energy Range from 20 to 310 meV

			m		
ionic state	orbital	character	20−50 meV	50−100 meV	100−310 meV
$X^2\Pi$	3π	$S_{3p} - O_{2p}$	-0.34 ± 0.01	-0.22 ± 0.01	-0.18 ± 0.01
$A^2\Pi$	2π	π_{CO}	-0.27 ± 0.06	-0.06 ± 0.06	0.02 ± 0.05
$B^2\Sigma^+$	9σ	S_{3s}	-0.35 ± 0.03	-0.11 ± 0.04	0.05 ± 0.03
$C^2\Sigma^+$	8σ	σ_{CO}	-0.56 ± 0.04	-0.38 ± 0.05	0.03 ± 0.04

As can be seen in Figure 2 and Table 1, CEDPICS for $X^2\Pi$ ionic state shows a decreasing trend with the increase of the collision energy E_c (negative E_c dependence) in the whole collision-energy range ($m = -0.34$ (E_c: 20−50 meV), −0.22 (E_c: 50−100 meV), and −0.18 (E_c: 100−310 meV)). In the low collision energy range from 20 to 50 meV, CEDPICS for $C^2\Sigma^+$ ionic state has found to show the most negative slope value of m (−0.56). It is well-known that negative E_c dependence of ionization cross section in lower collision energies can be related to the attractive interaction between a target and a He* metastable atom.[55,56] In fact, assuming Langevin-type cross section, the ionization cross section $\sigma(E_c)$ for atomic targets is proportional to $E_c^{-2/s}$,[55,56] if the radial dependence of an isotropic interaction potential $V^*(R)$ is expressed by $-CR_{-s}$ at long ranges (C is a constant). In the case of anisotropic molecular targets, Penning ionization processes are strongly dependent on the electron density distribution of the target MOs to be ionized. Therefore, in view of the observed negative CEDPICS for $X^2\Pi$ and $C^2\Sigma^+$ ionic states, dominant attractive potential wells in the present system are expected to exist around the regions where the electron density of the corresponding MOs (3π for $X^2\Pi$, and 8σ for $C^2\Sigma^+$) largely distributes. It should be noted that 3π MO has a large extent of the electron distribution in the sulfur atom side, while for 8σ MO the electrons largely distribute around the oxygen atom side. In addition, due to their orbital symmetries, the spatial extending regions of the electron distributions are different from each other; the perpendicular direction to the molecular axis (O−C−S) for 3π MO, while the collinear direction to the molecular axis for 8σ MO (see the electron density contour maps in Figures 1 and 2).

For the ionic states of $A^2\Pi$ and $B^2\Sigma^+$, relatively small collision energy dependence has been observed in the higher E_c range above ca. 100 meV ($m = 0.02$ for $A^2\Pi$, and 0.05 for $B^2\Sigma^+$ in the E_c range from 100 to 310 meV). In higher E_c regions, repulsive interaction between a target and a He* atom plays a significant role in the collisional ionization processes;[21,57] the ionization cross sections are expected to be larger as collision energy increases, since a faster He* atom can reach more effectively the reactive region against the repulsive wall, which results in a large overlap between relevant orbitals, than a slower He* atom. In this case, effective steepness of the repulsive wall in the interaction potential has found to be decisively important to characterize collision energy dependence of the ionization cross section.[21] Thus, it is supposed that the observed small E_c dependence is related to repulsive nature of the interaction

TABLE 2: Optimized Parameters of the Coefficients *Ci* in Equation 5, Obtained Potential Well Depths D_e, and Their Geometrical Positions of (R_e, θ_e) for OCS + He*(2^3S)

C_7/meV	2
C_6/meV	28
C_5/meV	159
C_4/meV	3906
C_3/meV	3555
C_2/meV	−1195
C_1/meV	54
D_e(O)/meV[a]	91
R_e(O)/Å[a]	3.5
θ_e(O)/deg[a]	26
D_e(S)/meV[b]	61
R_e(S)/Å[b]	2.9
θ_e(S)/deg[b]	111

[a] The well depth D_e around the O atom and its geometrical positions of R and θ. [b] The well depth D_e around the S atom and its geometrical positions of R and θ.

potential around the regions where the electron distributions of the corresponding MOs (2π for $A^2\Pi$, and 9σ for $B^2\Sigma^+$) largely extend.

In summary, the observed CEDPICS suggests that the interaction potential for OCS + He*(2^3S) is highly anisotropic. In section IV.B, anisotropy of the interaction potential will be discussed in detail.

B. Anisotropic Interaction of OCS with a He* Metastable Atom. The optimized potential parameters of C_i for the correction of Li model potential V_0 in eq 5 are summarized in Table 2. In the occupied MOs, the coefficients C_i except for C_2 show positive values. As discussed in the previous studies,[30−33] contributions of the positive coefficients for occupied MOs supplement 2s−2p hybridization effects,[21,57−59] which are underestimated in the Li model potential V_0 due to the larger energy gap between the 2s and 2p orbitals of the Li atom (1.848 eV) than that of He*(2^3S) (1.114 eV). The relatively large negative value (−1195 meV) of the optimized coefficient C_2 is somewhat confusing; however, it is supposed that this feature is caused by a subtle balance of many factors in evaluating highly anisotropic interaction as the present system. The coefficients C_i for the unoccupied MOs (C_5-C_7) are found to be positive, which are consistent with the previous studies.[30−33] The relative ratio between the optimized $K^{(i)}$ parameters associated with the ionization width for producing respective ionic states $\Gamma^{(i)}$ in eq 7 is found to be $K^{(X)}:K^{(A)}:K^{(B)}:K^{(C)} = 1.0:2.2:7.1:15.8$. The increasing trend for $K^{(i)}$ with respect to the ionization potentials for the respective ionic states has been discussed in the previous studies.[30−33,60]

Figure 3 shows a contour map of the optimized V^* for OCS + He*(2^3S). In the contour map, solid and dashed lines show positive and negative energy area, respectively. The energy spacing of the contour lines for negative values is 10 meV in the energy range from −80 to −10 meV. In the case of positive values, the energy spacing is 100 meV in the energy range from 0 to 800 meV. In Figure 4, the potential energy curves of $V^*(R)$ in several configurations are shown with solid lines; (a) the C═O bond side (θ = 0, 15, 60, and 90°) and (b) the C═S bond side (θ = 105, 120, 150, and 180°). As can be seen in Figures 3 and 4, it is interesting to note that attractive potential wells around the O and S atoms are clearly different in their directions. Around the O atom, an attractive potential region is found to extend in the collinear direction, while around the S atom, an attractive potential well is found to surround the molecular axis like a ring. The well depths D_e around the O atom and the S atom, and their geometrical positions of R_e and θ_e in the optimized V^* are listed in Table 2. In the O atom side, D_e(O), R_e(O), and θ_e(O) are found to be 91 meV (ca. 2.1 kcal/mol), 3.5 Å, and 26°, respectively. The attractive well depth and its positions around the S atom side D_e(S), R_e(S), and θ_e(S) are found to be 61 meV (ca. 1.4 kcal/mol), 2.9 Å, and 111°, respectively. As can be seen in Figure 4, the collinear side near the O atom (θ = 0°) is very attractive, whereas the collinear side around the S atom (θ = 180°) is rather repulsive with a very weak attractive well (ca. 10 meV). This difference can be related to the nature of interactions between He*(2^3S) and OCS, where the 2s−2p hybridization effects in the He*(2^3S) atom[21,57−59] is responsible for reducing repulsive interactions and increasing attractive interactions. As mentioned previously,[30] an electric polarization with the negative side in the outward direction is caused by the s−p hybridization effect on the He*(2^3S) atom. This yields a strong attractive interaction with the bond-dipole with a negative sign on the nearest atom in the target molecule. Permanent electric dipole moment of OCS was reported to be 0.72 D with partially negative charge on the O atom.[61] Natural population analysis by using the density functional theory with a standard B3LYP potential and 6-311+G* basis set also confirmed that the O atom in OCS has a −0.42 negative charge (the C and S atoms have +0.38 and +0.04 positive charges, respectively). Therefore, the above attractive interaction is likely to occur near the O atom. On the other hand, in the S atom, high energy levels of degenerate nonbonding 3p orbitals directed vertical to the C═S axis give attractive interactions in perpendicular directions.

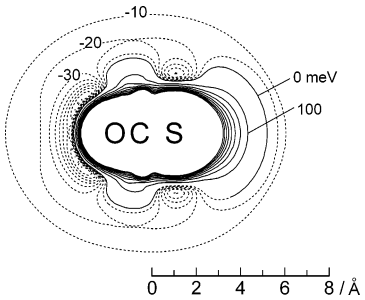

Figure 3. Contour map of the optimized potential V^* for OCS + He*-(2^3S) system. Positive and negative values of the potential energy are shown with solid lines and dotted lines, respectively. The energy spacing of the contour lines for negative value is 10 meV for the energy range from −80 to −10 meV. In the case of positive values, the energy spacing is 100 meV for the energy range from 0 to 800 meV.

In summary, for the attractive interaction of OCS with a He* atom it is concluded that the collinear approach is preferred in the O atom side, while the perpendicular approach is favored in the S atom. To obtain deeper insight into collisional ionization dynamics, theoretical simulations utilizing the optimized V^* have been performed. In section IV C, ionization probabilities as a function of the impact parameter b (opacity functions) are presented for $X^2\Pi$ and $C^2\Sigma^+$ ionic states to examine trajectories leading to ionization.

C. Opacity Functions for Producing $X^2\Pi$ and $C^2\Sigma^+$ Ionic States. Concerning with the attractive-site preference in the O and S atoms mentioned above, here we will focus our attention on $X^2\Pi$ and $C^2\Sigma^+$ ionic states. In Figures 5 and 6, calculated opacity functions for various trajectories at collision energies of 20, 50, 100, and 30 meV are shown for $X^2\Pi$ and $C^2\Sigma^+$ ionic states, respectively. For molecular targets, ionization probabilities depend on the molecular rotational motion and orientation as well as the impact parameter b, thus, a large number of dots appear at a particular value of b. The sum of the partial ionization probabilities $P^{(i)}$ for each trajectory cannot exceed the unity, this results in limited values of $P^{(i)}$ in the opacity

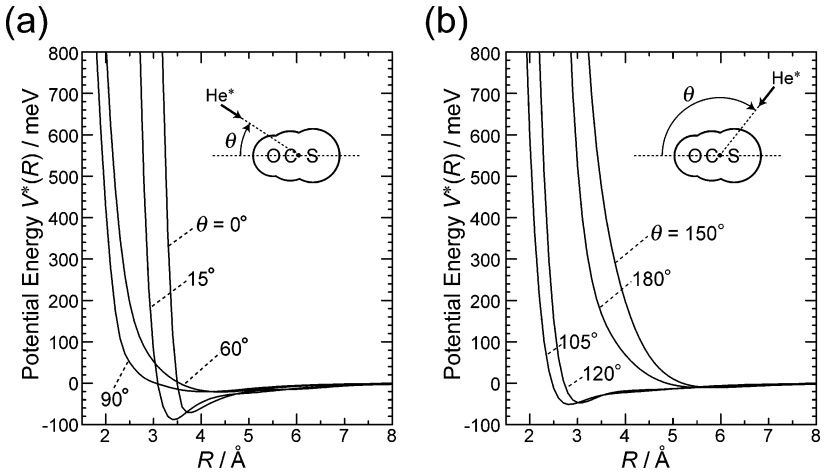

Figure 4. Optimized interaction potential energy curves of $V^*(R)$ as functions of distance R between He* and the center of mass of OCS for several directional approaches in (a) the C═O bond side (θ = 0, 15, 60, and 90°) and (b) the C═S bond side (θ = 105, 120, 150, and 180°).

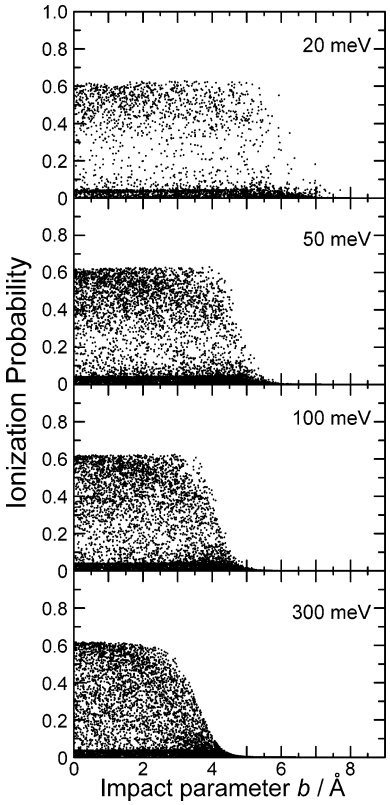

Figure 5. Ionization probabilities as a function of the impact parameter b (opacity function) for producing the $X^2\Pi$ ionic state of OCS at E_c = 20, 50, 100, and 300 meV.

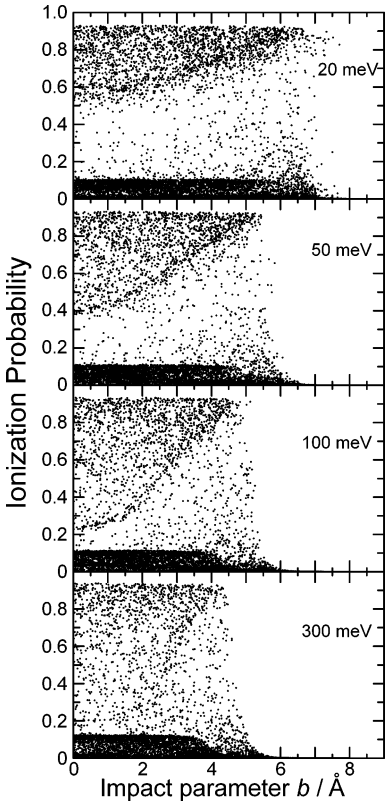

Figure 6. Ionization probabilities as a function of the impact parameter b (opacity function) for producing $C^2\Sigma^+$ ionic state of OCS at E_c = 20, 50, 100, and 300 meV.

functions. Penning ionization probabilities are distributed between a certain upper bound and a lower one. The trajectories near the upper bound are most reactive, leading to ionization into the corresponding ionic states, and those near the lower bound are least reactive.

The opacity functions largely depend on collision energy. This can be related to collisional ionization dynamics. For both ionic states, characteristic features in the opacity functions are summarized as follows.

(1) The critical impact parameter b_c rapidly decrease as the collision energy increases from 20 to 300 meV; for the $X^2\Pi$ state b_c = ca. 6.0, 4.5, 3.5, and 3.0 Å at E_c = 20, 50, 100, and 300 meV, respectively. For the $C^2\Sigma^+$ state b_c = ca. 7.5, 5.5, 5.0, and 4.5 Å at E_c = 20, 50, 100, and 300 meV, respectively.

(2) The upper boundary of the ionization probabilities is almost independent of the impact parameter less than the critical impact parameter b_c, while the ionization probabilities rapidly decrease when impact parameter exceeds the b_c.

These characters are connected to the negative collision energy dependence for both partial ionic states and can be understood in terms of the theoretical treatment for a spherical attractive potential.[55,56] For $b < b_c$, trajectories are mainly governed by the attractive potential and close collisions leading to ionization can occur. In this case, the ionization probability is almost independent of b. On the other hand, for $b > b_c$ reactive collisions cannot occur due to centrifugal barrier. Since the b_c decreases as collision energy increases, negative collision energy dependence can be expected. For anisotropic molecular

target of OCS, the trajectories that lead to collisional ionization into $X^2\Pi$ and $C^2\Sigma^+$ states with high probability are mainly governed by the attractive potential around S and O atom, respectively, since the large amount electron density of the corresponding MOs are most distributed in the attractive region.

As can be seen in Figures 5 and 6, ionization probability for $X^2\Pi$ and $C^2\Sigma^+$ state is limited to ca. 0.61 and 0.92, respectively. For $X^2\Pi$ state, the corresponding MO (3π) has a large extent of electron distribution perpendicular to the S atom; thus, trajectories that result in the upper boundary in Figure 5 can be related to collisional ionization around this region. However, ionization leading to a $A^2\Pi$ or $B^2\Sigma^+$ state also occurs to some extent since the corresponding MOs (2π and 9σ) have a small but certain electron distribution in the perpendicular direction to the S atom, which can limit the ionization probability for the $X^2\Pi$ state. On the other hand, for the $C^2\Sigma^+$ state the corresponding MO (8σ) has a large extent of electron distribution collinear to the O atom. Trajectories yielding the upper boundary in Figure 6 can be related to collisional ionization around this region. In this case, except for the 8σ MO, only the 9σ MO has electron density distribution in the σ-direction to the O atom, as can be seen in the electron density contour maps in Figures 1 and 2. Since the electron density of 9σ MO distributes very slighly in the collinear direction to the O atom, the ionization probability for $B^2\Sigma^+$ state is likely to be much lower than that for the $C^2\Sigma^+$ state. Thus, the limitation of the ionization probability for the $C^2\Sigma^+$ state is much higher than that for $X^2\Pi$ state.

It is interesting to note that the opacity functions for both ionic states are also characterized by some trajectories leading to considerably low ionization probabilities; ca. 0.05 and 0.1 for the $X^2\Pi$ and $C^2\Sigma^+$ states, respectively. As can be seen in Figures 1 and 3, for the $X^2\Pi$ state the corresponding MO (3π) has also a little electron density distribution around the O atom. This indicates that ionization into the $X^2\Pi$ state can also occur with a certain ionization probability around the O atom. However, its probability is expected to be much suppressed since 2π and 8σ MOs have a large extent of the electron density distribution around the same spatial region. For the $C^2\Sigma^+$ state, the corresponding MO 8σ has also a little electron density distribution in the collinear direction to the S atom, where the 9σ MO has a large extent of electron density distribution. Therefore, ionization into the $B^2\Sigma^+$ state predominantly occurs in the σ-direction around the S atom, which results in low ionization probability for the $C^2\Sigma^+$ state in this region.

V. Conclusion

Anisotropic interaction of OCS with a He*(2^3S) metastable atom has been investigated by collision-energy-resolved Penning ionization electron spectroscopy in a wide collision energy range from 20 to 350 meV. From the experimental data and the theoretical simulations based on classical trajectory calculations, the interaction potential for the OCS−He*(2^3S) system has been obtained. It is found that attractive potential wells around the O and S atoms are clearly different in their directions. Around the O atom, an attractive potential region is found to extend in the collinear direction (the well depth is ca. 90 meV), while around the S atom, an attractive potential well with a depth of ca. 40 meV is found to surround the molecular axis like a ring. This difference can be related to the nature of interactions between He*(2^3S) and OCS. Around the O atom, the 2s−2p hybridization of He* atom yields a strong attractive interaction with the bond-dipole, while in the S atom, high energy levels of degenerate nonbonding 3p orbitals directed vertical to the C═S axis give attractive interactions in perpendicular directions.

Collisional ionization dynamics in the chemiionization process was also investigated on the basis of the optimized potential energy surface and theoretical simulations. Opacity functions for producing $X^2\Pi$ and $C^2\Sigma^+$ ionic states are presented and can be explained in terms of the potential energy surface and the electron density distribution of molecular orbitals to be ionized.

Acknowledgment. The present work was supported by a Grant in Aid for Scientific Research from the Japanese Ministry of Education, Culture, Sports, Science, and Technology. T.H. and S.M. are supported by the Research Fellowship of the Japan Society for the Promotion of Science for Young Scientists.

References and Notes

(1) Stolte, S.; Suits, A.; Linnartz, H. *Chem. Phys.* **2004**, *301*, 159; a special issue on Stereodynamics of Molecular Reactions.
(2) Aquilanti, V.; Bartolomei, M.; Pirani, F.; Cappelletti, D.; Vecchiocattivi, F.; Shimizu, Y.; Kasai, T. *Phys. Chem. Chem. Phys.* **2005**, *7*, 291.
(3) Kramer, K. H.; Bernstein, R. B. *J. Chem. Phys.* **1965**, *42*, 767.
(4) Brooks, P. R.; Jones, E. M. *J. Chem. Phys.* **1966**, *45*, 3449.
(5) Stolte, S. *Ber. Bunsen-Ges. Phys. Chem.* **1982**, *86*, 413.
(6) Sinha, M. P.; Caldwell, C. D.; Zare, R. N. *J. Chem. Phys.* **1974**, *61*, 491.
(7) Pullman, D. P.; Herschbach, D. R. *J. Chem. Phys.* **1989**, *90*, 3881.
(8) Aquilanti, V.; Ascenzi, D.; Cappelletti, D.; Pirani, F. *Nature (London)* **1994**, *371*, 399.
(9) Pirani, F.; Cappelletti, D.; Bartolomei, M.; Aquilanti, V.; Scotoni, M.; Vescovi, M.; Ascenzi, D.; Bassi, D. *Phys. Rev. Lett.* **2001**, *86*, 5035.
(10) Penning, F. M. *Naturwissenschaften* **1927**, *15*, 818.
(11) Hotop, H.; Niehaus, A. *Z. Phys.* **1969**, *228*, 68.
(12) Čermák, V. *J. Chem. Phys.* **1966**, *44*, 3781.
(13) Yencha, A. J. In *Electron Spectroscopy: Theory, Techniques and Applications*; Brundle, C. R., Baker, A. D., Eds.; Academic: New York, 1984; Vol. 5.
(14) Ohno, K.; Mutoh, H.; Harada, Y. *J. Am. Chem. Soc.* **1983**, *105*, 4555.
(15) Ohno, K.; Matsumoto, S.; Harada, Y. *J. Chem. Phys.* **1984**, *81*, 4447.
(16) de Vries, M. S.; Tyndall, G. W.; Cobb, C. L.; Martin, R. M. *J. Chem. Phys.* **1987**, *86*, 2653.
(17) Ohoyama, H.; Kawaguchi, H.; Yamato, M.; Kasai, T.; Brunetti, B. G.; Vecchiocattivi, F. *Chem. Phys. Lett.* **1999**, *313*, 484.
(18) Okada, S.; Ohoyama, K. T. *Chem. Phys. Lett.* **2002**, *355*, 77.
(19) Okada, S.; Ohoyama, K. T. *J. Chem. Phys.* **2003**, *119*, 7131.
(20) Mitsuke, K.; Takami, T.; Ohno, K. *J. Chem. Phys.* **1989**, *91*, 1618.
(21) Ohno, K.; Takami, T.; Mitsuke, K.; Ishida, T. *J. Chem. Phys.* **1991**, *94*, 2675.
(22) Takami, T.; Mitsuke, K.; Ohno, K. *J. Chem. Phys.* **1991**, *95*, 918.
(23) Ohno, K. *Bull. Chem. Soc. Jpn.* **2004**, *77*, 887 and references therein.
(24) Nakamura, H. *J. Phys. Soc. Jpn.* **1969**, *26*, 1473.
(25) Miller, W. H. *J. Chem. Phys.* **1970**, *52*, 3563.
(26) Albertí, M.; Lucas, J. M.; Brunetti, B.; Pirani, F.; Stramaccia, M.; Rosi, M.; Vecchiocattivi, F. *J. Phys. Chem. A* **2000**, *104*, 1405.
(27) Biondini, F.; Brunetti, B. G.; Candori, P.; De Angelis, F.; Falcinelli, S.; Tarantelli, F.; Pirani, F.; Vecchiocattivi, F. *J. Chem. Phys.* **2005**, *122*, 164308.
(28) Ishida, T. *Chem. Phys. Lett.* **1992**, *1*, 191.
(29) Ishida, T.; Horime, K. *J. Chem. Phys.* **1996**, *105*, 5380.
(30) Maeda, S.; Yamazaki, M.; Kishimoto, N.; Ohno, K. *J. Chem. Phys.* **2004**, *120*, 781.
(31) Horio, T.; Yamazaki, M.; Maeda, S.; Hatamoto, T.; Kishimoto, N.; Ohno, K. *J. Chem. Phys.* **2005**, *123*, 194308.
(32) Horio, T.; Hatamoto, T.; Maeda, S.; Kishimoto, N.; Ohno, K. *J. Chem. Phys.* **2006**, *124*, 104308.
(33) Yamazaki, M.; Maeda, S.; Kishimoto, N.; Ohno, K. *J. Chem. Phys.* **2005**, *122*, 044303.
(34) Čermák, V. *J. Electron Spectrosc. Relat. Phenom.* **1976**, *9*, 419.
(35) Brion, C. E.; Yee, D. S. C. *J. Electron Spectrosc. Relat. Phenom.* **1977**, *12*, 77.
(36) Kishimoto, N.; Osada, Y.; Ohno, K. *J. Phys. Chem. A* **2000**, *104*, 1393.
(37) Kishimoto, N.; Osada, Y.; Ohno, K. *J. Electron Spectrosc. Relat. Phenom.* **2001**, *114−116*, 183.
(38) Kishimoto, N.; Horio, T.; Maeda, S.; Ohno, K. *Chem. Phys. Lett.* **2003**, *379*, 332.
(39) Yamakita, Y.; Tanaka, H.; Maruyama, R.; Yamakado, H.; Misaizu, F.; Ohno, K. *Rev. Sci. Instrum.* **2000**, *71*, 3042.
(40) Ohno, K.; Yamakado, H.; Ogawa, T.; Yamata, Y. *J. Chem. Phys.* **1996**, *105*, 7536.

(41) Rothe, E. W.; Neynaber, R. H.; Trujillo, S. *J. Chem. Phys.* **1965**, *42*, 3310.
(42) Hotop, H. *Radiat. Res.* **1974**, *59*, 379.
(43) Haberland, H.; Lee, Y. T.; Siska, P. E. *Adv. Chem. Phys.* **1981**, *45*, 487.
(44) Hotop, H.; Roth, T. E.; Ruf, M.-W.; Yencha, A. J. *Theor. Chem. Acc.* **1996**, *100*, 36.
(45) Frisch, M. J.; Trucks, G. W.; Schlegel, H. B.; et al. *Gaussian 94*, revision C.3; Gaussian, Inc.: Pittsburgh, PA, 1995.
(46) Boys, S. F.; Bernardi, F. *Mol. Phys.* **1970**, *19*, 553.
(47) Allan, C. J.; Gelius, U.; Allison, D. A.; Johansson, G.; Siegbahn, H.; Siegbahn, K. *J. Electron Spectrosc. Relat. Phenom.* **1972**, *1*, 131.
(48) Potts, A. W.; Williams, T. A. *J. Electron Spectrosc. Relat. Phenom.* **1972**, *3*, 3.
(49) Delwiche, J.; Hubin-Franskin, M. J.; Caprace, G.; Nitalis, P.; Roy, D. *J. Electron Spectrosc. Relat. Phenom.* **1980**, *21*, 205.
(50) Wang, L. S.; Reutt, J. E.; Lee, Y. T.; Shirley, D. A. *J. Electron Spectrosc. Relat. Phenom.* **1988**, *47*, 167.
(51) Holland, D. M. P.; Macdonald, M. A. *Chem. Phys.* **1990**, *114*, 279.
(52) Leung, K. T.; Brion, C. E. *Chem. Phys.* **1985**, *96*, 241.
(53) Cook, J. P. D.; White, M. G.; Brion, C. E.; Domcke, W.; Schirmer, J.; Cederbaum, L. S.; von Niessen, W. *J. Electron Spectrosc. Relat. Phenom.* **1981**, *22*, 261.
(54) Ehara, M.; Ishida, M.; Nakatsuji, H. *J. Chem. Phys.* **2002**, *117*, 3248.
(55) Bell, K. L.; Dalgarno, A.; Kingston, A. E. *J. Phys. B* **1968**, *1*, 18.
(56) Niehaus, A. *Adv. Chem. Phys.* **1981**, *45*, 399.
(57) Cohen, J. S.; Lane, N. F. *J. Chem. Phys.* **1977**, *66*, 586.
(58) Isaacson, A. D.; Hickman, A. P.; Miller, W. H. *J. Chem. Phys.* **1977**, *67*, 370.
(59) Siska, P. E. *J. Chem. Phys.* **1979**, *71*, 3942.
(60) Yamazaki, M.; Maeda, S.; Kishimoto, N.; Ohno, K. *J. Chem. Phys.* **2002**, *117*, 5707.
(61) Dijkerman, H. A.; Ruitenberg, G. *Chem. Phys. Lett.* **1969**, *3*, 172.